Chemical Engineering Journal 530 (2026) 173307

Contents lists available at ScienceDirect

Chemical Engineering Journal

journal homepage: www.elsevier.com/locate/cej

Achieving BT.2020 red emission with narrowband deep-red iridium complexes in OLEDs

Gyeong Seok Lee [a,1], Woo Jin Jeong [b,1], Huanyu Zhou [b], Hyun-Wook Kim [b], Da In Kim [a], Kwan-Nyeong Kim [b], Dong-Hyeok Kim [b], Thi Na Le [a], Seungyeon Cho [e], Jongchan Kim [e,f], Tae-Woo Lee [b,c,d,*], Yun-Hi Kim [a,*]

[a] Department of Chemistry and Research Institute for Molecular Alchemy, Gyeongsang National University, Jinju, 52828, Republic of Korea
[b] Department of Materials Science and Engineering, Seoul National University, Seoul, 08826, Republic of Korea
[c] Institute of Engineering Research, Interdisciplinary Program in Bioengineering, Research Institute of Advanced Materials, Soft Foundry, Seoul National University, Seoul, 08826, Republic of Korea
[d] SN Display Co., Ltd., Seoul, Seoul, 08826, Republic of Korea
[e] Department of Integrated Display Engineering, Yonsei University, Seoul, 03722, Republic of Korea
[f] Department of Electrical and Electronic Engineering, Yonsei University, Seoul, 03722, Republic of Korea

ARTICLE INFO

Keywords:
Red Ir-complex
Achieving BT.2020
Deep-red emissions
Narrowband red emission
Horizontal orientation

ABSTRACT

Achieving deep-red emission that meets the stringent BT.2020 color standard remains a critical challenge for phosphorescent organic light-emitting diodes (OLEDs). Here, we report two newly designed Iridium (Ir) (III) complexes, Ir(6-PhIqXy)$_2$dend and Ir(7-PhIqXy)$_2$dend, which incorporate a 1-(3,5-dimethylphenyl)-phenyl-isoquinoline ligand to enhance electron density, extend π-conjugation, and promote a planar molecular geometry favorable for horizontal dipole orientation. The newly designed Ir(III)-based emitters exhibit high photoluminescent quantum yields of 79.1% and 80.1%, deep-red emission peaks at 635 and 637 nm, and narrow full widths at half maximum (FWHMs) of 47 and 50 nm, respectively. Furthermore, the introduction of the ligand results in a high horizontal dipole ratio of 90.7% for Ir(6-PhIqXy)$_2$dend, leading to efficient light outcoupling and a maximum external quantum efficiency (EQE) of 19.1% without spectral broadening. Importantly, OLEDs incorporating both emitters exhibit ultra-narrowband deep-red emission peaking at 641 nm with a FWHM of 49 nm, yielding Commission Internationale de l'Éclairage (CIE) coordinates of (0.705, 0.294), which is the closest match to the BT.2020 red standard (0.708, 0.292) reported to date among Ir(III) - or Platinum(II)-based OLEDs. This work demonstrates that rational ligand engineering in Ir(III)-based phosphorescent emitters can concurrently achieve BT.2020-level color purity and high efficiency, providing a promising strategy for next-generation ultra-high-definition OLED displays.

1. Introduction

The continuous advancements in molecular design and device architecture have propelled organic light-emitting diodes (OLEDs) from academic exploration to thriving commercial success. With the growing demand for ultrahigh-resolution displays, enhancing the intrinsic color purity of organic emitters while maintaining high efficiency and long-term operational stability has become a crucial research focus. However, achieving high color purity remains challenging, as current commercial emitters, particularly phosphorescent materials, often exhibit broad full-width at half maximum (FWHM), leading to significant deviations of their Commission Internationale de l'Éclairage (CIE) coordinates from the BT.2020 standard.

The recent advances in multi-resonance (MR) emitters have shown great promise for achieving pure-red emission satisfying BT.2020 standards through molecular designs that minimize structural relaxation and enhance electron donation, thereby narrowing the emission spectrum [1]. Nevertheless, synthesizing MR emitters that combine high efficiency with uncompromised color purity remains a significant challenge. Among various emissive materials, Iridium(III) complexes

* Corresponding authors.
E-mail addresses: twlees@snu.ac.kr (T.-W. Lee), ykim@gnu.ac.kr (Y.-H. Kim).
[1] Gyeong Seok Lee and Woo Jin Jeong contributed equally to this work.

https://doi.org/10.1016/j.cej.2026.173307
Received 27 November 2025; Received in revised form 9 January 2026; Accepted 21 January 2026
Available online 21 January 2026

(hereafter referred to as Ir-complexes) have attracted considerable attention owing to their high efficiency and facile wavelength tunability, outperforming conventional fluorescent and thermally activated delayed fluorescence (TADF) materials [2–26]. However, the inherently broad emission spectra of these Ir-complexes pose a major challenge in realizing pure-red emission with precise color coordinates. The required redshift in emission often enhances charge-transfer characteristics, which undesirably broadens the spectrum and degrades color purity. For example, P. T. Chou and co-workers reported bis-tridentate Ir-complexes exhibiting a high external quantum efficiency (EQE) of 27.4% for red OLEDs. Due to their intrinsic multiple emission peaks, these emitters suffered from insufficient color purity, resulting in relatively poor CIE coordinates of (0.63, 0.38), which deviate from the BT.2020 red standard [24]. Later, Subsequently, Z. Wu and co-workers developed asymmetric Ir-complexes incorporating isoquinoline cyclometalating ligands and a thianthrene-5,5,10,10-tetraoxide ancillary moiety. These emitters delivered deep-red emission at 640 nm with an EQE of 25.8%. Nevertheless, the broad emission bandwidth led to unfavorable chromaticity coordinates of (0.68, 0.30), limiting their suitability for ultra-high-color-gamut displays [25]. In contrast, G.-G. Shan et al. introduced Ir-complexes featuring nitrogen-modulated cyclometalating ligands, achieving ultra-deep-red emission (675 nm) with CIE coordinates of (0.72, 0.27). Despite the favorable chromaticity, the corresponding OLEDs exhibited a relatively low EQE of 9.12% [26]. These imply that achieving both moderately high EQE in deep-red region and favorable CIE that meet BT.2020 standard is still challenging [27–30].

Therefore, in this study, we present newly designed Ir(III) complexes, namely Ir(6-PhIqXy)$_2$dend and Ir(7-PhIqXy)$_2$dend, which incorporate a 1-(3,5-dimethylphenyl)-phenylisoquinoline chelating ligand to enhance electron density, extends π-conjugation, and promotes a planar molecular geometry favorable for horizontal dipole alignment. These features enable deep-red emission from both emitters with CIE coordinates of (0.705, 0.294), nearly identical to the BT.2020 red standard (0.708, 0.292). Additionally, Ir(6-PhIqXy)$_2$dend achieves a high horizontal dipole orientation ratio of 90.7%, resulting in efficient light outcoupling and an EQE of 19.1% without spectral broadening. This work demonstrates, for the first time, that our newly designed Ir(III)-based red complexes can simultaneously deliver moderately high efficiency and strict BT.2020-level color purity, offering molecular-level insight into dipole orientation control through rational ligand design.

2. Results and discussion

2.1. Synthesis

The Ir-complexes were synthesized using the synthetic route shown in Scheme 1. The novel Ir-complexes, Ir(6-PhIqXy)$_2$dend and Ir(7-PhIqXy)$_2$dend, which use 3,7-diethylnonane-4,6-dione as an ancillary ligand, were developed using 1-(3,5-dimethylphenyl)-6-phenylisoquinoline and 1-(3,5-dimethylphenyl)-7-phenylisoquinoline as main ligands, respectively, to enhance their horizontal orientation in the excited states as well as the controlled color purity for BT2020. Based on consecutive synthetic procedure, two Ir-complexes were obtained in moderate yields of 80% and 84%. These complexes have been fully

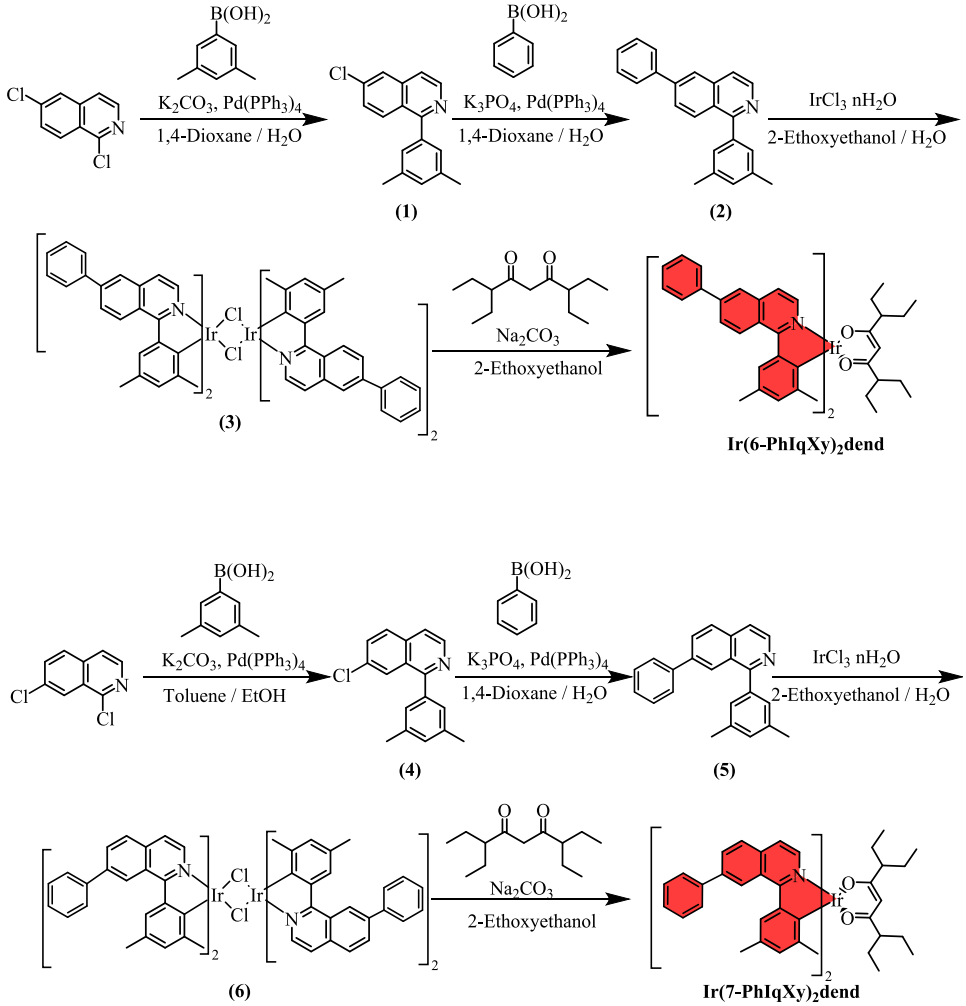

Scheme 1. The synthesis procedure of Ir(6-PhIqXy)$_2$dend (top) and Ir(7-PhIqXy)$_2$dend (bottom).

characterized by nuclear magnetic resonance (NMR) spectroscopy and high-resolution mass. The details of synthesis and characterization data are given in the Supporting Information (see Figs. S1–S18).

2.2. Theoretical calculations and photophysical properties

The electronic structures of the newly designed Ir-complex emitters were investigated using density functional theory (DFT) and time-dependent DFT (TD-DFT) calculations with the Schrödinger program. The optimized singlet and triplet geometries (Fig. 1a–b) with simulated singlet/triplet energy (S_1/T_1) of 2.02/1.62 eV for Ir(6-PhIqXy)$_2$dend and 2.10/1.70 eV for Ir(7-PhIqXy)$_2$dend, respectively. Both complexes exhibit identical energy levels for highest occupied molecular orbital (HOMO, −5.44 eV) and similar values for the lowest unoccupied molecular orbital (LUMO) energy (−2.82 eV for Ir(6-PhIqXy)$_2$dend and −2.84 eV for Ir(6-PhIqXy)$_2$dend) (Fig. 1c–d).

The LUMO and LUMO+1 of Ir(6-PhIqXy)$_2$dend are delocalized over one main ligand via the Ir atom and partially extend to the other main ligand. In contrast, Ir(7-PhIqXy)$_2$dend exhibits more localized LUMO distributions confined to a single main ligand. Additionally, the HOMO and HOMO-1 in Ir(6-PhIqXy)$_2$dend are also more delocalized on both Ir center and adjacent ligand region (Fig. S19). These promote stronger metal-ligand orbital mixing and enhanced MLCT (metal-to-ligand charge transfer) character in Ir(6-PhIqXy)$_2$dend compared to Ir(7-PhIqXy)$_2$dend. Natural transition orbital (NTO) analysis confirms that T_1 states are dominated by a single hole → particle transition (NTO weights >99%) (Fig. 1e–f). For both emitters, the electron NTO is mainly localized on the π* orbitals of the ligands, indicating ligand-centered electron excitation. In contrast, the hole NTOs differ significantly. Ir(6-PhIqXy)$_2$dend shows relatively higher Ir contribution with more hole NTO distribution at Ir center, indicative of stronger MLCT character in the T_1 state. Meanwhile, Ir(7-PhIqXy)$_2$dend exhibits a more ligand-localized hole NTO with reduced Ir participation, suggesting a more ligand-centered dominated excited state character with weaker MLCT mixing. Consistent with these observations, calculation of spin-orbit coupling matrix element (SOCME) showed that Ir(6-PhIqXy)$_2$dend possessed a larger SOCME between T_1 and S_o, ($\langle T_1|\hat{H}_{SOC}|S_o\rangle = 1.71$ cm^{-1} vs. 1.57 cm^{-1}), favoring efficient triplet radiative decay.

The UV–visible absorption and photoluminescence (PL) spectra of Ir(6-PhIqXy)$_2$dend and Ir(7-PhIqXy)$_2$dend in dichloromethane solution (room temperature and low temperature) and in vacuum-deposited thin films (TCTA:Ir-complexes (4%, 5 nm)/TPBi:Ir-complexes (3%, 5 nm)) are shown in Fig. 2a–c and summarized in Table 1. The strong absorption band below 450 nm corresponds to spin-allowed π-π* transitions, while the weaker band in the 500–650 nm region arises from a mixture of singlet and triplet metal-to-ligand charge transfer (^{1}MLCT and ^{3}MLCT) with additional inter-ligand charge transfer (^{1}ILCT) contributions. Particularly, the MLCT bands of Ir(6-PhIqXy)$_2$dend and Ir(7-PhIqXy)$_2$dend represent red-shifted absorption compared with reported quinoline-based Ir-complexes without an extended phenyl ring [27]. The optical band gaps were estimated to be 1.94 eV for Ir(6-PhIqXy)$_2$dend and 1.93 eV for Ir(7-PhIqXy)$_2$dend. These low optical bandgap energies had likely come from metal-induced strong spin-orbit coupling (SOC). This strong SOC partially relaxes spin selection rules, allowing forbidden $S_o \rightarrow T_1$ (^{3}MLCT) absorption with very low oscillator strength, and therefore, appearing weak absorption tails at long wavelength. Owing to the extended π-conjugation provided by the phenyl group on the quinoline ligand, both complex emitters exhibit deep-red emission, with PL maxima at 637 nm and a FWHM of 50 nm for Ir(6-PhIqXy)$_2$dend, while PL spectra for Ir(7-PhIqXy)$_2$dend peaked at 635 nm with slightly smaller FWHM of 47 nm. The more PL redshift in Ir(6-PhIqXy)$_2$dend could be attributed to the phenyl on the 6-position of quinoline directly extending the conjugated effect to the iridium complex. Importantly, these narrow emission bandwidths are due to the rigid molecular framework, where bulky phenyl and dendritic groups suppress vibrational relaxation and limit structural reorganization in the excited state. Interestingly, in doped TCTA:TPBi thin films, both Ir-complexes emit at ~638 nm with even narrower FWHMs (~42 nm,

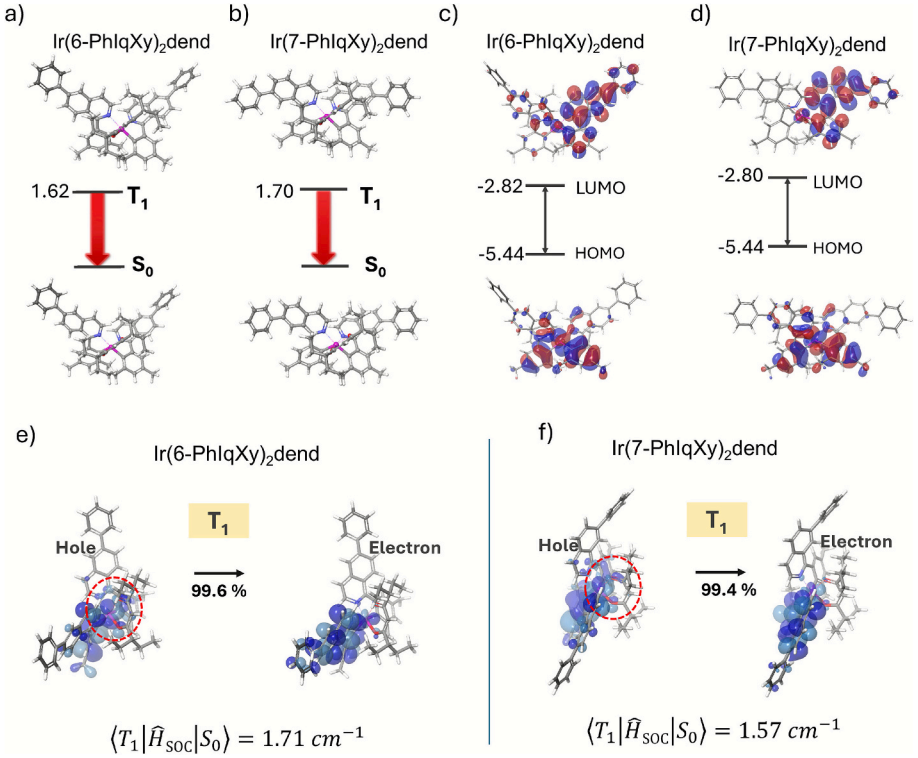

Fig. 1. Theoretical calculations and photophysical properties of newly designed Ir(6-PhIqXy)$_2$dend and Ir(7-PhIqXy)$_2$dend. (a) Optimized structure in singlet (S_1) and triplet (T_1) states. LUMO-HOMO distributions of (c) Ir(6-PhIqXy)$_2$dend and (d) Ir(7-PhIqXy)$_2$dend. NTO simulation with SOC calculations for (e) Ir(6-PhIqXy)$_2$dend and (f) Ir(7-PhIqXy)$_2$dend.

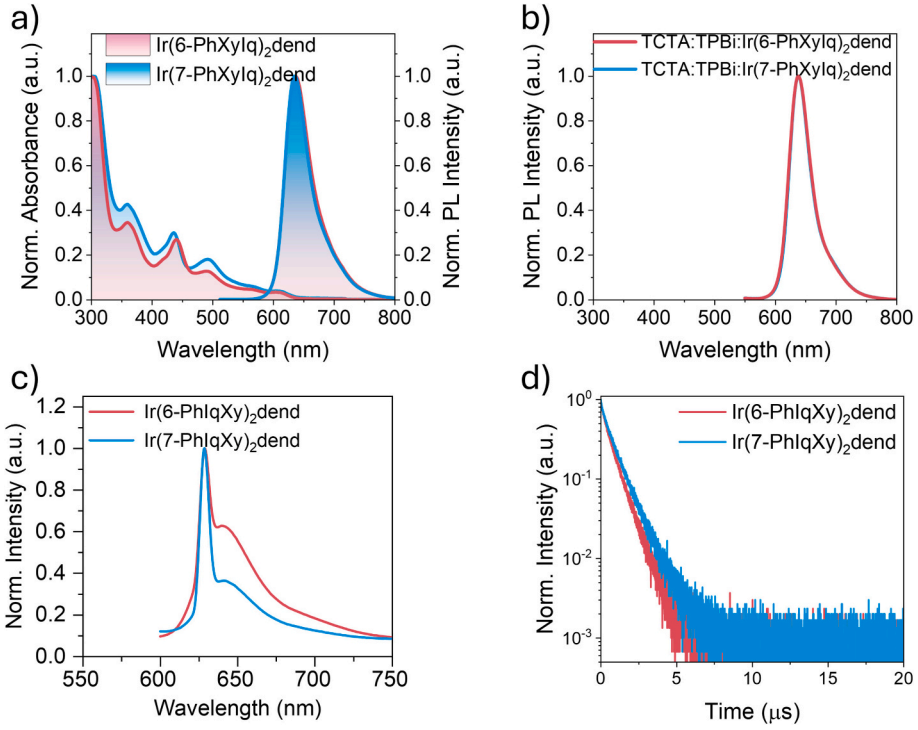

Fig. 2. Photophysical properties of Ir(6-PhIqXy)$_2$dend and Ir(7-PhIqXy)$_2$dend. (a) Normalized absorbance and PL intensity in dichloromethane solution at room temperature. (b) Normalized PL intensity of the two Ir-complex emitters when doped in mixed host TCTA:TPBi (film). (c) Normalized PL intensity at low temperature (77 K). (d) TRPL of the two Ir-complex emitters in solution state.

Table 1
Photophysical properties of Ir(6-PhIqXy)$_2$dend and Ir(7-PhIqXy)$_2$dend.

Ir-complex	UV–Vis[a] (nm)	PL peak[a] (nm)	FWHM[a] (nm)	E_{T1} (eV)	$E_{HOMO/LUMO}$[b] (eV)	τ_{ave} (ns)	Band gap[a] (eV)	Horizontal orientation (%)	PLQY (%)
Ir(6-PhIqXy)$_2$dend	359, 440, 492, 609	637	50.0	2.0	−5.06/−3.12	713	1.94	90.7	80.1
Ir(7-PhIqXy)$_2$dend	359, 436, 492, 610	635	47.0	2.0	−5.05/−3.12	873	1.93	86.6	79.1

[a] UV–vis absorption and photoluminescence (PL) spectra were measured in a 1×10^{-5} M DCM solution.
[b] The LUMO energy level was determined by cyclic voltammetry (CV) measured in a 1×10^{-5} M DMF solution.

Fig. 2b) without any shoulder peaks. The low-temperature PL (LTPL) indicates that both emitters have the same T_1 value as 2.0 eV (Fig. 2c). At low temperature, suppressed thermal motion and reduced homogeneous broadening allowed the vibronic transitions, which corresponded to shoulder peak, to become spectrally distinguishable. The broad tail emission in the LTPL spectra also suggests that Ir(6-PhIqXy)$_2$dend exhibits a slightly higher MLCT-to-LT ratio, which is consistent with simulation results. The PL of the two emitters in solvents with different polarity shows that both emitters have broadened spectra with increased polarity (Fig. S20).

In addition, time-resolved PL (TRPL) measurements of the vacuum-deposited films revealed average lifetimes (τ_{avg}) of 713 ns for Ir(6-PhIqXy)$_2$dend and 873 ns for Ir(7-PhIqXy)$_2$dend (Fig. 2d). The shorter exciton lifetime in Ir(6-PhIqXy)$_2$dend could be attributed to its slightly higher MLCT contribution and SOC values. These exciton lifetimes are significantly shorter than those of conventional phosphorescent emitters [31]. The vacuum-deposited emissive layers of Ir(6-PhIqXy)$_2$dend and Ir(7-PhIqXy)$_2$dend showed comparably high PL quantum yields (PLQYs) of 80.1% and 79.1%, respectively, implying nearly identical radiative efficiencies with minimal non-radiative trap-mediated losses. The coexistence of high PLQYs with sub-microsecond lifetimes suggests that the shortened τ_{avg} arises from efficient exciton transfer and radiative recombination rather than from enhanced non-radiative decay.

The two new Ir-complexes show identical LUMO of −3.12 eV and negligible difference in HOMO, which is −5.06 eV for Ir(6-PhIqXy)$_2$dend and − 5.05 eV for Ir(7-PhIqXy)$_2$dend (Fig. S21). The thermal stability of the Ir-complexes was assessed via thermogravimetric analysis (TGA) and differential scanning calorimetry (DSC) measurements (Fig. S22). A high decomposition temperature (T_d, defined at 5% weight loss) was recorded from TGA measurement to be 367 °C for Ir(6-PhIqXy)$_2$dend and 334 °C for Ir(7-PhIqXy)$_2$dend, while the DSC measurements showed no phase transitions up to 300 °C. These indicated the high thermal stability of our newly synthesized Ir-complexes.

2.3. Highly horizontal dipole oriented Ir-complex emitters

To gain deeper insight into the intrinsic molecular orientation behavior of the two new Ir-complexes, molecular dynamics (MD) simulations were performed by depositing 50 molecules of each Ir-complex onto a TAPC substrate, which serves as the hole-transporting layer in the device (Fig. 3a). The transition dipole moment (TDM) vectors were computed for each molecule, where blue and green vectors represent horizontally and vertically oriented components, respectively. The angle (θ) between each TDM vector and the substrate normal was used to calculate the orientation order parameter (S) (see Fig. 3a for definition). The orientation distributions are shown in Fig. 3b and c. Ir(6-

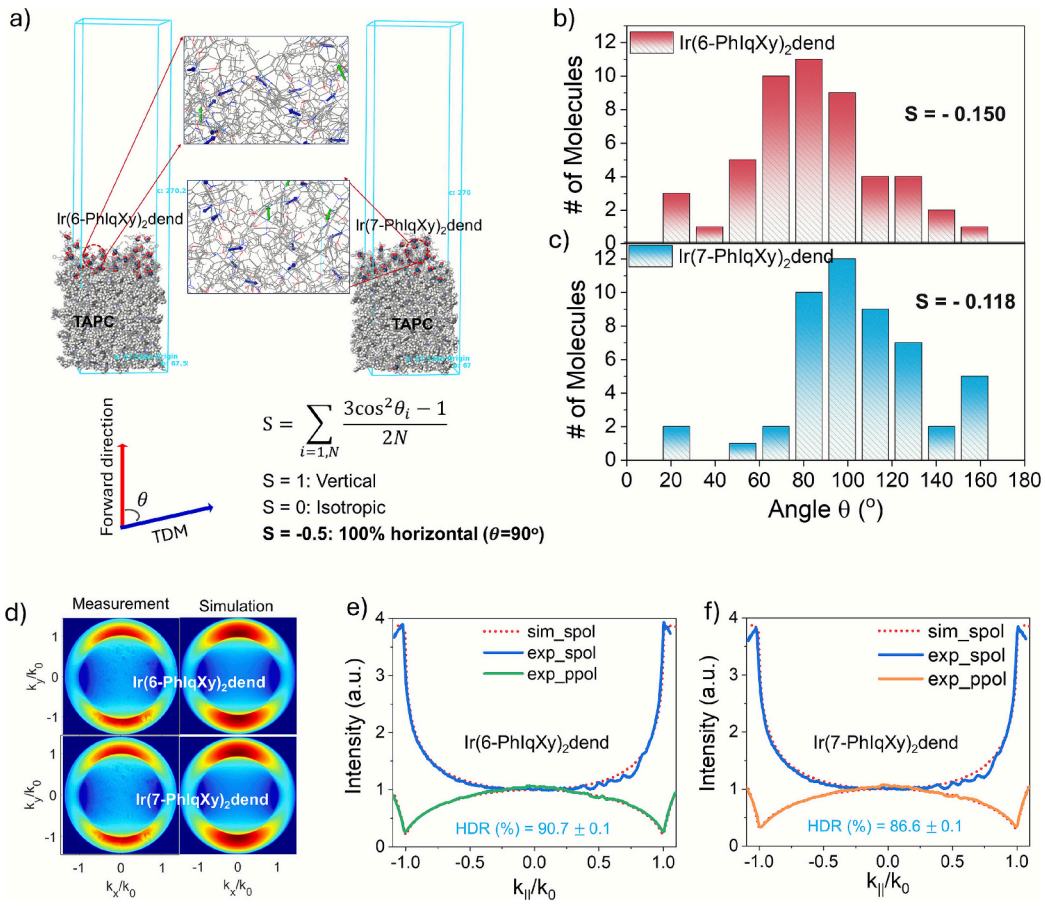

Fig. 3. a) Deposition of 50 Ir-complex molecules for each type of emitter on TAPC. The blue and green vectors represent the tendency for horizontal and vertical orientations, respectively. The equation for order parameter (S) with explanation for its values. The probability distributions of θ between the TDM vectors and the forward direction for b) Ir(6-PhIqXy)$_2$dend and c) Ir(7-PhIqXy)$_2$dend. d) FIM Simulation and measurement. Horizontal dipole ratio (HDR) results measured from FIM measurement for e) Ir(6-PhIqXy)$_2$dend and f) Ir(7-PhIqXy)$_2$dend.

PhIqXy)$_2$dend exhibited a more negative S value (S = -0.150) than Ir(7-PhIqXy)$_2$dend (−0.118), indicating a stronger horizontal alignment tendency for Ir(6-PhIqXy)$_2$dend. The relatively high simulated θ values for Ir(7-PhIqXy)$_2$dend implied that their TDMs for are tilted downward toward the TAPC substrate, whereas those of Ir(6-PhIqXy)$_2$dend are more preferred horizontal oriented with slightly upward from the substrate plane. This opposite tilting behavior originates from the distinct ligand substitution positions on the quinoline ligands, which influence both molecular symmetry and local dipole distribution (Fig. S23), affecting π–π and van der Waals interactions with the TAPC surface. Nevertheless, it is worth noting that molecular orientation also depends on factors such as the deposition rate and the type of substrate; therefore, slight discrepancies between the simulated and experimental results are common [32–34].

Despite their intrinsically three-dimensional and non-planar geometries, the chemical/geometrical asymmetry of our emitters could induce an anisotropy in molecular orientation. The larger aspect ratio γ for Ir(6-PhIqXy)$_2$dend (γ = 1.4) compared to Ir(7-PhIqXy)$_2$dend (γ = 1.2) indicates a more laterally extended (disk-like) molecular envelope, arising from the phenyl substituent at the 6-position compared to the 7-position (see Fig. S24). This increased lateral extension is expected to enlarge the intermolecular and host-guest interaction surface area, thereby favoring a face-on adsorption configuration during film formation and inducing a preferential horizontal orientation of the emitter molecules [35–37].

Additionally, we performed simulations of the TDM orientation of the Ir-complex emitters separately doped into the TCTA and TPBi hosts (Fig. S25). Both emitters exhibit a preferred horizontal orientation, as evidenced by their negative S values. The differences in S values for each emitter when doped in TCTA versus TPBi indicated that the molecular orientation of the emitter was strongly dependent on the host material. This behavior can likely be attributed to anisotropy in the electrostatic potential (ESP) of the emitters, which affects their van der Waals interactions with different host environments (Fig. S24) [30].

The dipole orientation of the new Ir-complexes, doped in bilayer (TCTA:Ir-complexes (4%, 5 nm)/TPBi:Ir-complexes (3%, 5 nm), was then experimentally determined using Fourier imaging microscopy (FIM) (Fig. 3d–f) and further validated with spectrally resolved FIM (SR-FIM) (Fig. S26) to ensure accuracy. In the Fourier (k-space) image, $k_x/k_0 = 0$ contains information solely about s-polarization, while $k_y/k_0 = 0$ reflects p-polarization. To separate the polarization modes of the emitted light, a linear polarizer was used to decompose the emission into orthogonal p- and s-polarized components, which were then analyzed with a spectrometer. By fitting these polarization-resolved measurements to optical simulations with varying horizontal dipole orientation ratios, the degree of horizontal dipole orientation in the emissive materials was determined. As a result, Ir(6-PhIqXy)$_2$dend and Ir(7-PhIqXy)$_2$dend exhibit very high horizontal dipole orientation ratios of 90.7% and 86.6%, respectively, which agrees with the tendency observed from simulation results. SR-FIM analysis yielded similar results, further confirming the reliability of our measurements. These highly horizontal orientation could be attributed to the excellent planarity in both Ir-complexes with rigid, oblate molecular structures, which promote strong π–π and van der Waals interactions, leading to preferential horizontal alignment during molecular stacking [35,38]. The different coordination environment between Ir(6-PhIqXy)$_2$dend and Ir(7-

PhIqXy)$_2$dend induced by the 6- and 7-position phenyl substitutions alter the steric environment around the iridium center and electronic effect at the iridium center. Specifically, the 6-phenyl substitution promoting a more symmetric and direct electronic effect to Ir center through the N of quinoline by conjugation, thereby enhancing overall molecular planarity and enhanced coordination bond compared to the 7-phenyl analogue [39,40]. The high horizontal dipole orientation is critical for light outcoupling, directing more emitted light toward the substrate and thereby increasing the EQE [29].

2.4. Electroluminescence properties with BT.2020 achievement

To exploit the high horizontal dipole orientation of Ir(6-PhIqXy)$_2$dend and Ir(7-PhIqXy)$_2$dend for enhanced OLED light outcoupling, vacuum deposition was preferred over solution processing, as spin-coating often results in random molecular orientations. Vacuum-deposited devices with the following structure were fabricated: ITO/GraHIL (90 nm)/TAPC (15 nm)/TCTA:Ir-complexes (1:0.4%, 5 nm) & TPBi:Ir-complexes (1:0.3%, 5 nm)/TPBi (55 nm)/LiF (2 nm)/Al (100 nm) (Fig. 4a). Here, an exciplex co-host composed of TCTA and TPBi, having closely aligned singlet and triplet energy levels along with reduced charge-trapping sites [28], was used to facilitate the efficient transfer of both singlet and triplet energies to Ir-complex emitters.

Device characteristics are presented in Figs. 4b–f and S27 and summarized in Table 2. Both devices exhibit similar low turn-on voltages (V_{on}) of 2.7 V. The luminance recorded at 9 V was 1992 cd·m^{-2} and 3386 cd·m^{-2}, respectively, in Ir(6-PhIqXy)$_2$dend and Ir(7-PhIqXy)$_2$dend devices. The lower luminance in Ir(6-PhIqXy)$_2$dend device was due to the lower current flowing in device, implying that the substituted positions had impact on the charge transport properties of the emitters. Nevertheless, the OLED based on Ir(6-PhIqXy)$_2$dend achieved a maximum EQE_{max} of 19.1% and a maximum current efficiency (CE_{max}) of 8.9 cd·A^{-1}, whereas the Ir(7-PhIqXy)$_2$dend device only reached 17.0% and 7.8 cd·A^{-1}. The EQEs at 100 cd·m^{-2} and 1000 cd·m^{-2} were 15.6% and 9.8% for Ir(6-PhIqXy)$_2$dend, 15.0% and 9.4% for Ir(7-PhIqXy)$_2$dend, respectively. Given the nearly identical photophysical properties and PLQYs, the improvement in device performance is primarily attributed to differences in horizontal dipole orientation rather than intrinsic emissive properties. The higher horizontal dipole ratio of Ir(6-PhIqXy)$_2$dend facilitates more efficient light outcoupling, enabling enhanced photon extraction from the OLED structure. Angular luminance measurements also reveal that devices exhibit angle-dependent emission closely following the Lambertian distribution. Additionally, the efficiency roll-off in both devices was attributed to the low T_1 of put deep red Ir-complex emitters. Such low-energy triplet excitons are intrinsically more susceptible to non-radiative quenching processes, which naturally leads to enhanced efficiency roll-off under high driving conditions. Nevertheless, our devices still exhibit state-of-the-art efficiency within the ultra-deep-red regime.

Both devices exhibit deep-red electroluminescent (EL) spectra peaking at 641 nm with a very narrow FWHM of 49 nm, resulting in highly pure red emission (Fig. 4c). At a luminance of 100 cd·m^{-2}, the

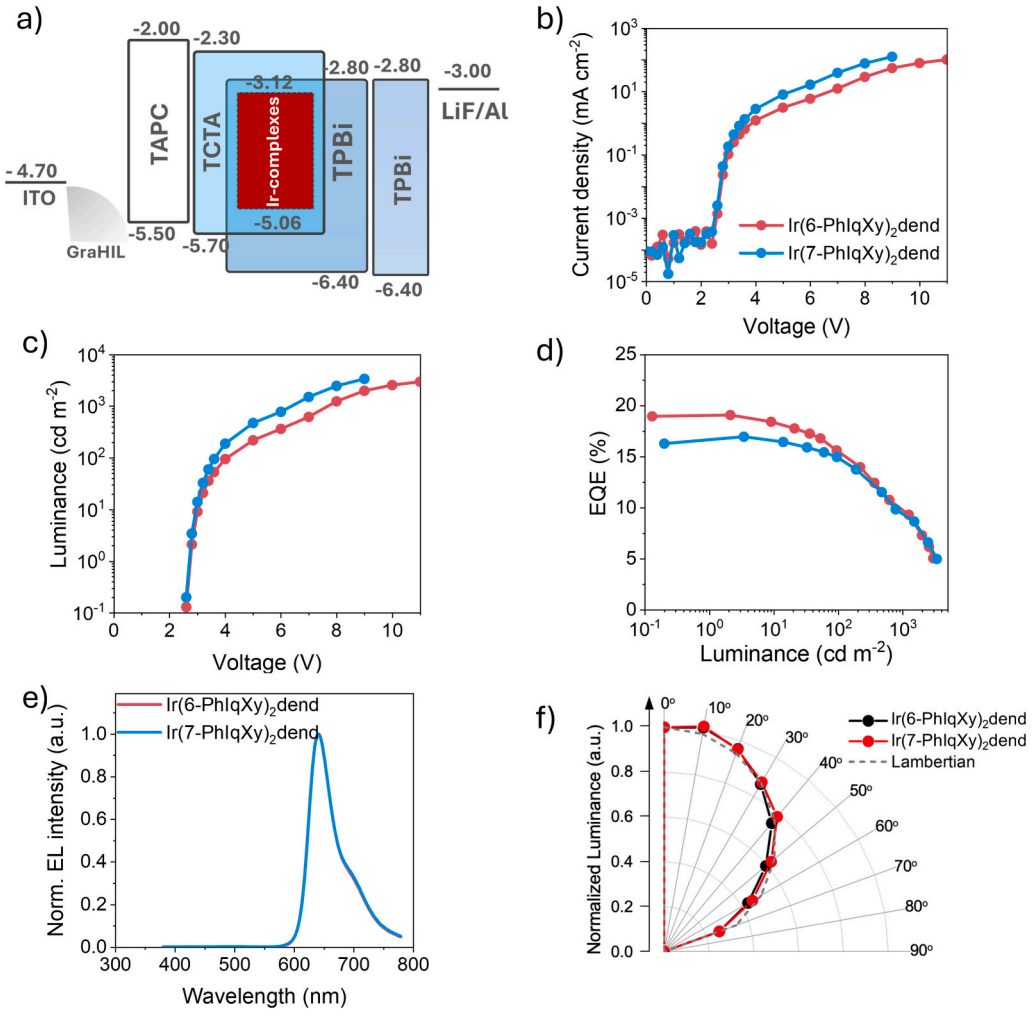

Fig. 4. a) Device structure with energy level diagram of OLED devices using newly synthesized Ir-complexes as emitters. Device characteristics: b) Current density - voltage graph, c) luminance - voltage, d) EQE - Luminance graph, e) normalized EL spectra, f) normalized angle-dependent EL.

Table 2
EL properties of Ir(6-PhIqXy)$_2$dend and Ir(7-PhIqXy)$_2$dend based OLEDs.

Emitter	V_{on} (V)	CE_{Max} (cd A^{-1})	$EQE_{Max/100/1000}$ (%)	FWHM (nm)	EL spectra (nm)	CIE (x, y)
Ir(6-PhIqXy)$_2$dend	2.7	8.9	19.1/15.6/9.8	49	641	(0.705, 0.294)
Ir(7-PhIqXy)$_2$dend	2.7	7.8	17.0/15.0/9.4	49	641	(0.705, 0.294)

devices show CIE (x, y) coordinates of (0.705, 0.294), which are nearly identical to the BT.2020 red standard of (0.708, 0.292) (Fig. 5a). To the best of our knowledge, this represents the first report of such characteristics in a phosphorescent red OLED. Comparative data with previously reported studies are presented as FWHM-wavelength, EQE-CIEx, and EQE-CIEy plots in Fig. 5b–d and summarized in Table S1. The FWHM obtained in this work is among the narrowest reported for red Ir-complex-based OLEDs (Fig. 5b).

Importantly, despite their moderately high EQE values, the CIEx and CIEy coordinates of our devices show the closest match to the BT.2020 red standard. In contrast, the coordinates of all previously reported references deviate significantly from the BT.2020 values (Fig. 5c–d). Importantly, this spectral precision is realized without sacrificing efficiency, as evidenced by the moderately high EQE values. Collectively, the combination of moderately high efficiency and outstanding color purity positions these newly designed narrowband deep red Ir-complexes as highly promising candidates for advanced OLED displays, particularly in premium applications where both energy efficiency and accurate color reproduction are essential.

3. Conclusion

In summary, we designed and synthesized Ir(III)-based pure red complexes for OLEDs that deliver deep-red emission, narrow FWHM, and low driving voltage, addressing key requirements for high-resolution display technology. The newly developed 1-(3,5-dimethylphenyl)-phenylisoquinoline chelating ligand enhances electron density and extends π-conjugation, thereby narrowing the energy gap to match the BT.2020 red region while also promoting a planar molecular geometry favorable for horizontal dipole alignment. Although Ir(6-PhIqXy)$_2$dend and Ir(7-PhIqXy)$_2$dend exhibit nearly identical excited-state energy levels, we identified horizontal dipole orientation as the

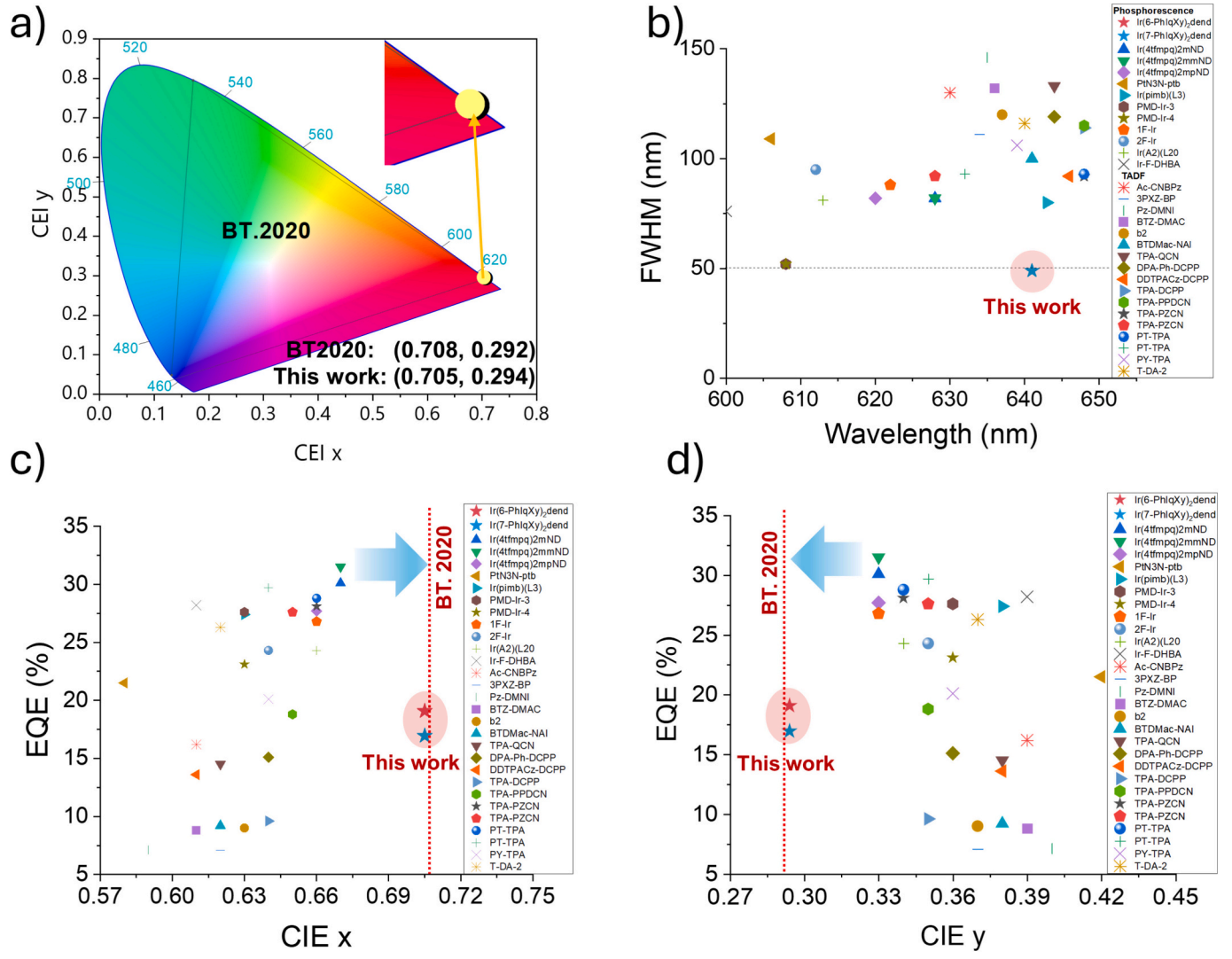

Fig. 5. a) Color coordinates of OLEDS using newly synthesized Ir-complexes compared to BT.2020 Standard red emission. b) FWHM - wavelength, c) EQE - CIEx, and d) EQE - CIEy of new Ir-complexes compared to literature reports about red OLEDs. The CIE coordinates were measured at 100 cd·m^{-2}.

decisive factor governing device efficiency. Ir(6-PhIqXy)$_2$dend achieved a higher orientation ratio of 90.7% compared to 86.6% for Ir(7-PhIqXy)$_2$dend, resulting in superior light outcoupling and an EQE of 19.1%. Notably, the two Ir-complexes also deliver precise color purity with CIE (x, y) coordinates of (0.705, 0.294), representing the closest match to the BT.2020 red standard among reported red phosphorescent OLEDs based on Ir(III) or Pt(II) complexes.

CRediT authorship contribution statement

Gyeong Seok Lee: Writing – original draft, Methodology, Data curation. **Woo Jin Jeong:** Methodology, Investigation, Data curation. **Huanyu Zhou:** Methodology, Data curation. **Hyun-Wook Kim:** Formal analysis, Data curation. **Da In Kim:** Data curation. **Kwan-Nyeong Kim:** Investigation. **Dong-Hyeok Kim:** Investigation. **Thi Na Le:** Writing – original draft, Software, Data curation. **Seungyeon Cho:** Investigation. **Jongchan Kim:** Writing – review & editing, Data curation. **Tae-Woo Lee:** Writing – review & editing, Supervision, Conceptualization. **Yun-Hi Kim:** Writing – review & editing, Supervision, Project administration, Investigation, Funding acquisition, Conceptualization.

Declaration of competing interest

The authors declare that they have no known competing financial interests or personal relationships that could have appeared to influence the work reported in this paper.

Acknowledgement

This research was supported by the National Research Foundation of Korea (RS-2024-00336766 and RS-2023-00301974) and by the Pioneer Research Center Program through the National Research Foundation of Korea funded by the Ministry of Science, ICT and Future Planning (RS-2022-NR067540) and Samsung Display.

Appendix A. Supplementary data

Supplementary data to this article can be found online at https://doi.org/10.1016/j.cej.2026.173307.

Data availability

No data was used for the research described in the article.

References

[1] T. Fan, M. Du, X. Jia, L. Wang, Z. Yin, Y. Shu, Y. Zhang, J. Wei, D. Zhang, L. Duan, High-efficiency narrowband multi-resonance emitter fusing indolocarbazole donors for BT. 2020 red electroluminescence and ultralong operation lifetime, Adv. Mater. 35 (2023) 2301018, https://doi.org/10.1002/adma.202301018.
[2] Y.-Y. Wang, K.-N. Tong, K. Zhang, C.-H. Lu, X. Chen, J.-X. Liang, C.-K. Wang, C.-C. Wu, M.-K. Fung, J. Fan, Positive impact of chromophore flexibility on the efficiency of red thermally activated delayed fluorescence materials, Mater. Horiz. 8 (2021) 1297–1303, https://doi.org/10.1039/D1MH00028D.
[3] S. Wang, X. Yan, Z. Cheng, H. Zhang, Y. Liu, Y. Wang, Highly efficient near-infrared delayed fluorescence organic light emitting diodes using a phenanthrene-based charge-transfer compound, Angew. Chem. Int. Ed. 54 (2015) 13068, https://doi.org/10.1002/anie.201506687.
[4] T. Yang, B. Liang, Z. Cheng, C. Li, G. Lu, Y. Wang, Construction of efficient deep-red/near-infrared emitter based on a large π-conjugated acceptor and delayed fluorescence OLEDs with external quantum efficiency of over 20%, J. Phys. Chem. C 123 (2019) 18585 https://doi.org/10.1021/acs.jpcc.9b05875.
[5] S. Wang, Z. Cheng, X. Song, X. Yan, K. Ye, Y. Liu, G. Yang, Y. Wang, Highly efficient long-wavelength thermally activated delayed fluorescence OLEDs based on dicyanopyrazino phenanthrene derivatives, ACS Appl. Mater. Interfaces 9 (2017) 9892–9901, https://doi.org/10.1021/acsami.6b14796.
[6] J.-L. He, F.-C. Kong, B. Sun, X.-J. Wang, Q.-S. Tian, J. Fan, L.-S. Liao, Highly efficient deep-red TADF organic light-emitting diodes via increasing the acceptor strength of fused polycyclic aromatics, Chem. Eng. J. 424 (2021) 130470, https://doi.org/10.1016/j.cej.2021.130470.
[7] F.-M. Xie, P. Wu, S.-J. Zou, Y.-Q. Li, T. Cheng, M. Xie, J.-X. Tang, X. Zhao, Efficient orange–red delayed fluorescence organic light-emitting diodes with external quantum efficiency over 26%, Adv. Electron. Mater. 6 (2020) 1900843 https://doi.org/10.1002/aelm.201900843.
[8] Q. Zhang, H. Kuwabara, W.J. Potscavage, S. Huang, Y. Hatae, T. Shibata, C. Adachi, Anthraquinone-based intramolecular charge-transfer compounds: computational molecular design, thermally activated delayed fluorescence, and highly efficient red electroluminescence, J. Am. Chem. Soc. 136 (2014) 18070–18081, https://doi.org/10.1021/ja510144h.
[9] T. Yang, Z. Cheng, Z. Li, J. Liang, Y. Xu, C. Li, Y. Wang, Improving the efficiency of red thermally activated delayed fluorescence organic light-emitting diode by rational isomer engineering, Adv. Funct. Mater. 30 (2020) 2002681, https://doi.org/10.1002/adfm.202002681.
[10] T. Chen, C.-H. Lu, C.-W. Huang, X. Zeng, J. Gao, Z. Chen, Y. Xiang, W. Zeng, Z. Huang, S. Gong, C.-C. Wu, C. Yang, Tuning the emissive characteristics of TADF emitters by fusing heterocycles with acridine as donors: highly efficient orange to red organic light-emitting diodes with EQE over 20%, J. Mater. Chem. C 7 (2019) 9087, https://doi.org/10.1039/C9TC01973A.
[11] C. Li, R. Duan, B. Liang, G. Han, S. Wang, K. Ye, Y. Liu, Y. Yi, Y. Wang, Deep-red to near-infrared thermally activated delayed fluorescence in organic solid films and electroluminescent devices, Angew. Chem. Int. Ed. 129 (2017) 11683–11687, https://doi.org/10.1002/ange.201706464.
[12] B. Wang, H. Yang, Y. Zhang, G. Xie, H. Ran, T. Wang, Q. Fu, Y. Ren, N. Sun, G. Zhao, J.-Y. Hu, Q. Wang, Highly efficient electroluminescence from evaporation- and solution-processable orange–red thermally activated delayed fluorescence emitters, J. Mater. Chem. C 7 (2019) 12321–12327, https://doi.org/10.1039/C9TC04418C.
[13] R. Furue, K. Matsuo, Y. Ashikari, H. Ooka, N. Amanokura, T. Yasuda, Highly efficient red–orange delayed fluorescence emitters based on strong π-accepting dibenzophenazine and dibenzoquinoxaline cores: toward a rational pure-red OLED design, Adv. Opt. Mater. 6 (2018) 1701147, https://doi.org/10.1002/adom.201701147.
[14] F. Ni, Z. Wu, Z. Zhu, T. Chen, K. Wu, C. Zhong, K. An, D. Wei, D. Ma, C. Yang, Teaching an old acceptor new tricks: rationally employing 2,1,3-benzothiadiazole as input to design a highly efficient red thermally activated delayed fluorescence emitter, J. Mater. Chem. C 5 (2017) 1363, https://doi.org/10.1039/C7TC00025A.
[15] Y. Wu, X. Chen, Y. Mu, Z. Yang, Z. Mao, J. Zhao, Z. Yang, Y. Zhang, Z. Chi, Two thermally stable and AIE active 1,8-naphthalimide derivatives with red efficient thermally activated delayed fluorescence, Dyes Pigments 169 (2019) 81–88, https://doi.org/10.1016/j.dyepig.2019.04.071.
[16] P. Halder, V. Talukdar, A. Iqubal, P. Das, Palladium-catalyzed aminocarbonylation of isoquinolines utilizing chloroform-COware chemistry, J. Org. Chem. 87 (2022) 13965–13979, https://doi.org/10.1021/acs.joc.2c01629.
[17] G.-Z. Lu, Q. Zhu, L. Liu, Z.-G. Wu, Y.-X. Zheng, L. Zhou, J.-L. Zuo, H. Zhang, Pure red iridium(III) complexes possessing good electron mobility with 1,5-naphthyridin-4-ol derivatives for high-performance OLEDs with an EQE over 31%, ACS Appl. Mater. Interfaces 11 (2019) 20192–20199, https://doi.org/10.1021/acsami.9b02558.
[18] B. Liang, Z. Yu, X. Zhuang, J. Wang, J. Wei, K. Ye, Z. Zhang, Y. Liu, Y. Wang, Achieving high-performance pure-red electrophosphorescent iridium(III) complexes based on optimizing ancillary ligands, Chem. Eur. J. 26 (2020) 4410, https://doi.org/10.1002/chem.201905690.
[19] P. Gnanasekaran, Y. Yuan, C.-S. Lee, X. Zhou, A.K.-Y. Jen, Y. Chi, Realization of highly efficient red phosphorescence from bis-tridentate iridium(III) phosphors, Inorg. Chem. 58 (2019) 10944, https://doi.org/10.1021/acs.inorgchem.9b01383.
[20] B. Jiang, C. Zhao, X. Ning, C. Zhong, D. Ma, C. Yang, Using simple fused-ring thieno [2,3-d]pyrimidine to construct orange/red Ir(III) Complexes: high-performance red organic light-emitting diodes with EQEs up to nearly 28%, Adv. Opt. Mater. 6 (2018) 1800108 https://doi.org/10.1002/adom.201800108.
[21] Z. Lua, Q. Lub, Y. Yanga, Z. Jianga, Q. Zenga, W. Zhoua, L. Juna, Y. Gonga, Y. Liua, Y. Miao, S. Guo, Solution-processed high-performance orange-red organic light-emitting diode (OLED) based on ionic phosphorescent iridium(III) complex, J. Organomet. Chem. 967 (2022) 122333, https://doi.org/10.1016/j.jorganchem.2022.122333.
[22] S.-N. Liu, K.-N. Tong, Y. Zhao, J.-F. Cheng, M.-K. Fung, J. Fan, Efficient red phosphorescent Ir(III) complexes based on rigid ligands with high external quantum efficiency and low efficiency roll-off, J. Mater. Chem. C 8 (2020) 6168, https://doi.org/10.1039/C9TC06940B.
[23] Y.-L. Zhang, Q. Ran, Q. Wang, Y. Liu, C. Hanisch, S. Reineke, J. Fan, L.-S. Liao, High-efficiency red organic light-emitting diodes with external quantum efficiency close to 30% based on a novel thermally activated delayed fluorescence emitter, Adv. Mater. 31 (2019) 1902368, https://doi.org/10.1002/adma.201902368.
[24] C. Kuei, W.L. Tsai, M. Jiao, W.K. Lee, Y. Chi, C.C. Wu, S.H. Liu, G.H. Lee, P.T. Chou, Bis-tridentate Ir(III) complexes with nearly unitary RGB phosphorescence and organic light-emitting diodes with external quantum efficiency exceeding 31%, Adv. Mater. 28 (2016) 2795, https://doi.org/10.1002/adma.201505790.
[25] Y. Sun, X. Yang, Z. Feng, B. Liu, D. Zhong, J. Zhang, G. Zhou, Z. Wu, Highly efficient deep-red organic light-emitting devices based on asymmetric iridium(III) complexes with the thianthrene 5,5,10,10-tetraoxide moiety, ACS Appl. Mater. Interfaces 11 (2019) 26152–26164, https://doi.org/10.1021/acsami.9b06749.
[26] L.-L. Wen, J.-M. Zhang, Y.-P. Han, Y.-C. Duan, W.-F. Xie, K.-Z. Shao, G.-G. Shan, Z.-M. Su, Boosting the efficiency of deep-red Ir(III) complexes by modulating nitrogen atoms for high-performance OLEDs, Inorg. Chem. Front. 11 (2024) 133–141, https://doi.org/10.1039/D3QI01824E.
[27] G.R. Han, O. Kwon, S. Kim, J. Choi, J.B. Son, K.S. Min, J.W. Lee, B. Choi, S.K. Kim, Investigation of the relationship between quantum yield, charge-transfer state, and structure of the ligands in red-emitting heteroleptic iridium(III) complexes, J. Phys. Chem. A 128 (2024) 6124–6131, https://doi.org/10.1021/acs.jpca.4c00914.

[28] J.Y. Woo, M.-H. Park, S.-H. Jeong, Y.-H. Kim, B. Kim, T.-W. Lee, Advances in solution-processed OLEDs and their prospects for use in displays, Adv. Mater. 35 (2022) 2207454, https://doi.org/10.1002/adma.202207454.
[29] C.-K. Moon, K.-H. Kim, J.-J. Kim, Unraveling the orientation of phosphors doped in organic semiconducting layers, Nat. Commun. 8 (2017) 791, https://doi.org/10.1038/s41467-017-00804-0.
[30] S. Kim, J.-M. Kim, J. Choi, M. Sim, Y. Koishikawa, Y.-S. Cho, S. Kim, S.-Y. Kwak, A. Jeon, O. Kwon, D.-H. Lee, J.Y. Lee, B. Choi, Rational ligand design of heteroleptic iridium (III) complexes toward nearly perfect horizontal dipole orientation for highly efficient red-emitting phosphorescent organic light-emitting diodes, Adv. Funct. Mater. 33 (2023) 2214233, https://doi.org/10.1002/adfm.202214233.
[31] Y.H. Jung, G.S. Lee, S. Muruganantham, H.R. Kim, J.H. Oh, J.H. Ham, S.B. Yadav, J.H. Lee, M.Y. Chae, Y.-H. Kim, J.H. Kwon, Modified t-butyl in tetradentate platinum (II) complexes enables exceptional lifetime for blue-phosphorescent organic light-emitting diodes, Nat. Commun. 15 (2024) 2977, https://doi.org/10.1038/s41467-024-47307-3.
[32] H.-D. Lee, H.J. Jang, J.H. Baek, J.-J. Kim, H.C. Choi, J.-M. Kim, J.Y. Lee, Preferred orientation evolution of hole transport materials for high emitting dipole orientation ratio of the emitting material, Adv. Optical Mater. 11 (2023) 2202109, https://doi.org/10.1002/adom.202202109.
[33] C. Bishop, Y. Li, M.F. Toney, L. Yu, M.D. Ediger, Molecular orientation for vapor-deposited organic glasses follows rate-temperature superposition: the case of posaconazole, J. Phys. Chem. B 124 (2020) 2505–2513, https://doi.org/10.1021/acs.jpcb.0c00625.
[34] C. Scherer, N. Kinaret, K.-H. Lin, M.N. Qaisrani, F. Post, F. May, D. Andrienko, Predicting molecular ordering in deposited molecular films, Adv. Energy Mater. 14 (2024) 2403124, https://doi.org/10.1002/aenm.202403124.
[35] M.C. Jung, J. Facendola, J. Kim, D.S.M. Ravinson, P.I. Djurovich, S.R. Forrest, M. E. Thompson, Molecular alignment of homoleptic iridium phosphors in organic light-emitting diodes, Adv. Mater. 33 (2021) 2102882, https://doi.org/10.1002/adma.202102882.
[36] M. Schmid, K. Harms, C. Degitz, T. Morgenstern, A. Hofmann, P. Friederich, H.-H. Johannes, W. Wenzel, W. Kowalsky, W. Brütting, Optical and electrical measurements reveal the orientation mechanism of homoleptic iridium-carbene complexes, ACS Appl. Mater. Interfaces 12 (2020) 51709, https://doi.org/10.1021/acsami.0c14613.
[37] K. Shi, C. Wu, H. Zhang, K.-N. Tong, W. He, W. Li, Z. Jin, S. Jung, S. Li, X. Wang, S. Gong, Y. Zhang, D. Zhang, F. Kang, Y. Chi, C. Yang, G. Wei, Enhanced emitting dipole orientation based on asymmetric iridium(III) complexes for efficient saturated-blue phosphorescent OLEDs, Adv. Sci. 11 (2024) 2402349, https://doi.org/10.1002/advs.202402349.
[38] S. Kuila, H. M.-Salinas, J. Eng, C. Li, M.R. Bryce, T.J. Penfold, A.P. Monkman, Rigid and planar π-conjugated molecules leading to long-lived intramolecular charge-transfer states exhibiting thermally activated delayed fluorescence, Nat. Commun. 15 (2024) 9611, https://doi.org/10.1038/s41467-024-53740-1.
[39] I.C.M. W.-Ooyevaar, G.M. Kapteijn, D.M. Grove, W.J.J. Smeets, A.L. Spek, G. V. Koten, Ligand substitution reactions in new square-planar iridium, rhodium and platinum complexes containing a potentially terdentate C,N,N' ligand system; crystal structure of [Ir{$C_6H_4CH_2N(Me)CH_2CH_2NMe_2$–2-C,N,N'}(cod)](cod = cycloocta-1,5-diene), J. Chem. Soc. Dalton Trans. (1994) 703–711, https://doi.org/10.1039/DT9940000703.
[40] K.-H. Kim, E.S. Ahn, J.S. Huh, Y.-H. Kim, J.-J. Kim, Design of heteroleptic Ir complexes with horizontal emitting dipoles for highly efficient organic light-emitting diodes with an external quantum efficiency of 38%, Chem. Mater. 28 (2016) 7505–7510, https://doi.org/10.1021/acs.chemmater.6b03428.